Numerical Study of the Flowfield in a Differentially-Throttled Linear Aerospike

(Article begins on next page)

25 December 2024

NUMERICAL STUDY OF THE FLOWFIELD IN A DIFFERENTIALLY-THROTTLED LINEAR AEROSPIKE

J. Hassan[1], R. Marsilio[1], G. M. Di Cicca[1] & M. Ferlauto[1]

[1]Department of Mechanical and Aerospace Engineering, Politecnico di Torino, Corso Duca degli Abruzzi 24, Turin, Italy

Abstract

Although bell-shaped nozzle is the only type of nozzles that is practically used in every space launch vehicle, space onboard-thrusters and other proplusive devices. However, multiple alternative designs of nozzle have been studied and are considered as promising alternatives due to their increased propulsive efficiency. One of these advanced nozzles is aerospike nozzle. The winning point of the design of such nozzle is the inherent capability of its exhaust being self-adaptable to external pressure. This adaptability gives it a competitive edge over other types of nozzles.

In the present numerical study, the flowfield of a linear aerospike nozzle is characterized. The nozzle plug is truncated to 20% of its ideal length. The Reynolds-averaged Navier–Stokes equations have been solved to predict the flowfield. The flowfield is studied in two modes of nozzle operation. The first mode is symmetric operation (non-differential throttling configuration), where the sub-nozzles on either side of the plug are subjected to the same incoming flow. In the second mode, the nozzle operates with asymmetric incoming flow conditions (differential throttling configuration); where each sub-nozzle, on either side of the plug, experiences different boundary conditions. The percent difference between the nozzle pressure ratios (NPR) of the sub-nozzles, one on each side of the plug, is termed as the differential factor (DF). For the non-differential throttling configuration, numerical simulations have been carried out for nozzle pressure ratios of 5, 50, and 200, at differential factor of 0%. Whereas, for the differential throttling configuration, numerical simulations have been conducted for nozzle pressure ratios of 5, 50 and 200, but each with differential factor of 10%, 25%, and 50%. The numerical results accurately characterize the flowfield around the linear aerospike nozzle in terms of Mach number contours and pressure distribution over the plug.

Keywords: Aerodynamics, Linear Aerospike Nozzle, Numerical, Differential Throttling

1. Background

Quest for inventions and discoveries has kept a prominent portion of humankind busy since its beginning. In the fields of science and engineering, quest of improving or negating the explanation of discovered phenomena and increasing the efficiency of engineered products have also kept sufficient numbers of research community busy in every period of humanity. Such willingness and dedication of individuals and groups led to Wright brothers' powered heavier-than-air aircraft flight in 1903 in USA, opening door to quick onward progress in Aeronautics, and to first artificial satellite successful launch from Earth through Sputnik rocket in 1957; thereby leading humanity towards successful manned spaceflights and galvanized the field of astronautics.

In addition to other fields, Aerodynamics and Propulsion have played significant roles in the success of aforementioned human feats in Aerospace arena. Successful vehicles in both Aeronautics and Astronautics are attributed to their efficient aerodynamic designs and propulsion systems designs. Nozzle is compulsory component of propulsion systems, which are based on jet technology e.g., turbojet engines, turbofan engines, Ramjets, Scramjets and, of course, rockets, and in wind tunnels. Therefore, nozzle has been the focus of researchers, especially from aerodynamic and propulsion aspects and others.
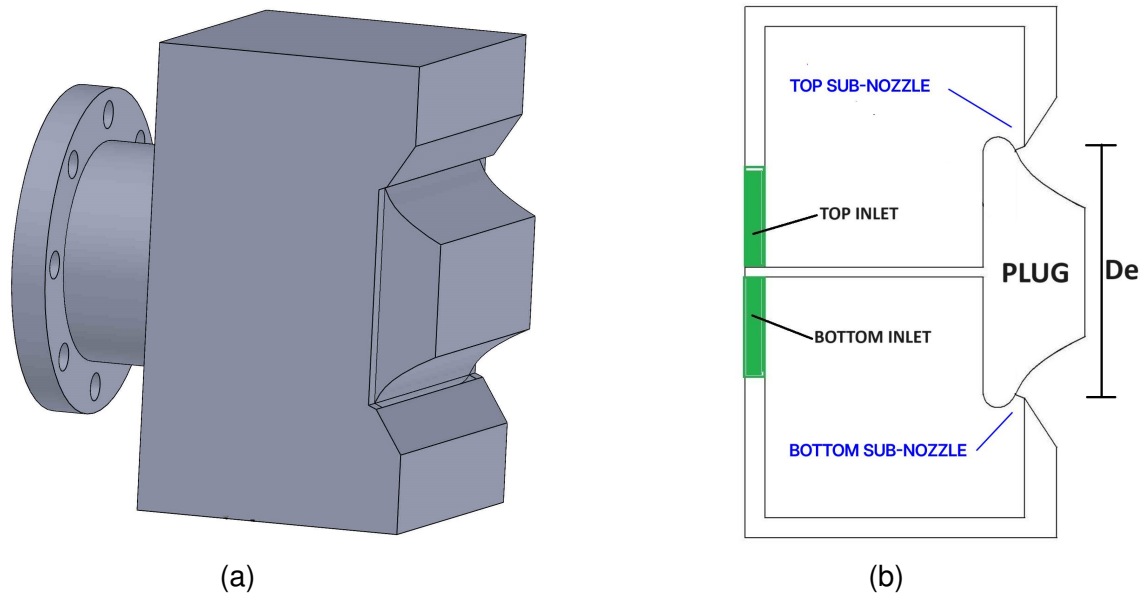
Figure 1 – (a) LASN20 3D model with its chamber and flow inlet, (b) 2D diagram of LASN20 with its chamber, in the symmetric plane

Currently, all the rockets and spacecrafts, which travel to space and some travel back, have rocket engines with traditional bell-shaped nozzles which are basically convergent-divergent nozzles. This traditional bell-shaped nozzle operates at maximum efficiency at its design point. At off-design conditions, it operates either in over-expanded or under-expanded form. As Aeronautics community is in pursuit of renascence of civilian aircraft aerodynamics by researching beyond tube-and-wings aircraft into blended-wing-body (BWB) and/or hybrid-wing-body aircrafts configuration [1]; in the same way, researchers from astronautics and aeronautics are also in pursuit of efficient nozzle by eliminating or minimizing the over-expanded and under-expanded instabilities [2, 3, 4, 6, 7]. Resultantly, plug nozzle has been proposed as one of the alternative solutions to achieve higher performance at both design and off-design conditions.

Unlike bell nozzles, the flow is free to expand along the plug, as it is no longer surrounded by solid boundaries on its outside. Therefore, plug nozzles can adapt to different altitudes by expanding the flow to ambient pressure, resulting in continuous altitude-adaptation [10]. Due to high surface area that needs to be cooled, introduction of aerospike geometry, which is essentially a truncated plug nozzle, has helped mitigate cooling issue [11]. Aerospike nozzles have also been presented as a solution for Single-Stage-To-Orbit or clustered launchers owing to their self-adapting capability [12].

Understanding and improving the aerodynamic characteristics of such nozzles has been the subject of numerous theoretical, experimental and numerical studies [8], [9]. With limited usability of rocket control surfaces as it ascends from thinner-air to space, rockets rely on additional systems for maneuvering during its trajectory; either by use of additional thrusters or gimbaling primary rocket engine(s) or differential throttling in presence of multiple traditional rocket engines. For such thrust-vectoring [13], researchers have also focused on fluidic thrust vectoring [14] to minimize the number of hardware in propulsion system. In rocket engines with plug / aerospike nozzle, differential throttling is also achieved by varying the exhaust from the sub-nozzles, i.e. the nozzles composing the clustered plug [15, 16].

In this computational study, two-dimensional flowfield of linear aerospike nozzle with 20% plug is characterized. Reynolds-averaged Navier–Stokes equations have been solved for the prediction of the flowfield, using commercially available software of computational fluid dynamics. This flowfield is obtained in two modes of nozzle operation. The first mode is symmetric operation (non-differential throttling configuration) where the sub-nozzles on either side of the plug are subjected to similar incoming flow, while the second mode operates with asymmetric incoming flow conditions (differential
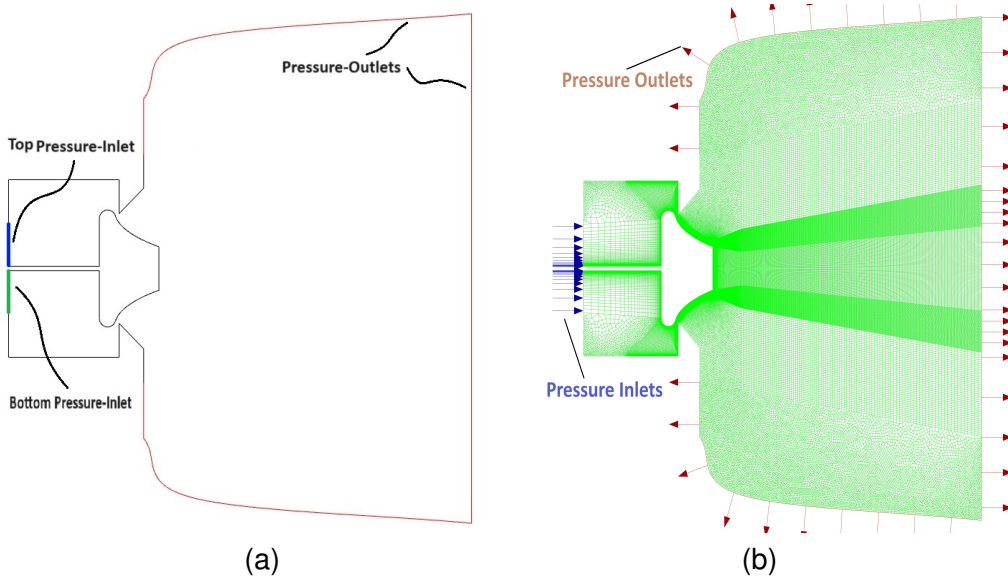
(a)

(b)

Figure 2 – (a) Boundaries of computational domain (b) Domain mesh

throttling configuration) where each sub-nozzle on either side of the plug is at different boundary conditions.

The percent difference between the nozzle pressure ratios (NPR) of the sub-nozzles, one on each side of the plug, is termed as the differential factor (DF), where DF = 0% represents symmetric operation. For the non-differential throttling configuration, numerical simulations have been carried out for NPR = 5, 50, and 200, at DF = 0%. Whereas, for the differential throttling configuration, numerical simulations have been conducted at NPR = 5, 50 and 200, each with DF = 10%, 25%, and 50%. The numerical results correctly characterize the flowfield around linear aerospike nozzle in terms of mach contours and pressure distribution over the surfaces of plug which is 20% of its ideal length.

2. Computational Details

The flow inside a propulsive nozzle is compressible with high pressure gradients. Numerical simulations of such flow require a compressible, viscous and turbulent flow model in computational fluid dynamics (CFD).

The flow governing equations adopted in present work are the compressible, steady Reynolds-Averaged Navier-Stokes equations (RANS). The compact integral form of unsteady Reynolds-Averaged Navier-Stokes equations (URANS) is written as:

$$\frac{\partial}{\partial t}\int_v \vec{W}\,d\mathcal{V} + \int_{\mathcal{S}} \vec{F}_I \cdot \hat{n}\,d\mathcal{S} + \int_{\mathcal{S}} \vec{F}_V \cdot \hat{n}\,d\mathcal{S} = \int_{\mathcal{V}} \vec{H}\,d\mathcal{V} \tag{1}$$

in an arbitrary volume $\mathcal{V}$ enclosed in a surface $\mathcal{S}$. With usual conventions, $\vec{W} = \{\rho, \rho\vec{q}, E, \tilde{v}_t\}^T$ is the hyper-vector of conservative variables, $\vec{F}_I$ and $\vec{F}_V$ are tensors containing the inviscid and the viscous fluxes, respectively.

$$\vec{F}_I = \left\{ \rho\vec{q}, p\bar{\bar{I}} + \rho\vec{q}\otimes\vec{q}, (E+p)\vec{q}, \tilde{v}_t\vec{q} \right\}^T, \tag{2}$$

$$\vec{F}_V = \left\{ 0, -\bar{\bar{\tau}}, -\kappa\nabla T - \bar{\bar{\tau}}\cdot\vec{q}, -\frac{\nu+\tilde{v}_t}{\sigma}\nabla\tilde{v}_t \right\}^T \tag{3}$$

$\vec{q} = \{u, v, w\}^T$ is the velocity vector, E the total energy per unit volume, M_∞ and Re_∞ are the free-stream Mach number and the Reynolds number, γ is the ratio of the specific heats and $\bar{I}$ is the unit matrix. The term $\vec{H}$

$$\vec{H} = \left\{ 0, 0, 0, c_{b1}\tilde{S}\tilde{v}_t + \frac{c_{b2}}{\sigma_3}(\nabla\tilde{v}_t)^2 - c_{w1}f_w\left(\frac{\tilde{v}_t}{d}\right)^2 \right\}^T \tag{4}$$

contains turbulence model source terms.

The viscous stresses are

$$\tau_{ij} = (\mu + \mu_t) \left[\frac{\partial q_j}{\partial x_i} + \frac{\partial q_i}{\partial x_j} - \frac{2}{3} (\nabla \cdot \vec{q}) \delta_{ij} \right] \tag{5}$$

The laminar viscosity μ is computed via the Sutherland's law, whereas the turbulent viscosity $\mu_t = \rho \nu_t$ is defined according to the Spalart-Allmaras (S-A) model [18]. Despite its simplicity, the S-A model has shown a close agreement with the experimental data for the case of unsteady nozzle flow, as shown in a comparative study involving 14 different turbulence models [20].

This study has been carried out using ANSYS-Fluent RANS density-based solver, by using a second order accurate finite volume discretization and implicit pseudo time stepping[17]. As mentioned above, the Spalart-Allmaras model has been used as the turbulence model has been selected for accounting of turbulence effects. This model has been successfully employed by other researchers for turbulence modeling of aerospike flow [22, 12]. A flux-vector splitting scheme of Advection Upstream Splitting Method (AUSM) has been selected for implicit formulation of the solution. The AUSM scheme first computes a cell interface Mach number based on the characteristic speeds from the neighboring cells. The interface Mach number is then used to determine the upwind extrapolation for the convection part of the inviscid fluxes. A separate Mach number splitting scheme is used for the pressure terms [17]. All the computations have been performed by using the steady solver, so that the system of governing equations is over-relaxed to the steady state.

2.1 Nozzle Model

A linear aerospike nozzle, with a plug of 20% of its ideal length, has been used for numerical computations. This nozzle, figure 1, has nozzle-throat width to height ratio of 30.41. Its other dimensions are tabulated in table 1. Its sub-nozzles have sonic exit Mach number, M_e, while its plug contours are designed based on a method proposed in reference [23]. It has been designed for nozzle pressure ratio, NPR_{design} = 200.

2.2 Meshing and Boundary Conditions

The two-dimensional domain, figure 2, is the symmetric plane of 3D nozzle model geometry from figure 1(a), albeit with no inlet circular duct. Its 2D mesh contains 0.127 million cells and is shown in figure 2(b).

This linear aerospike nozzle model has been taken from reference [24, 25] but with a plug of 20% of its ideal length. For symmetric mode of operation, both the top and bottom inlets are subjected to NPR = 5, 50 and 200. For asymmetric mode of operations, NPR at the bottom inlet NPR_{Bottom} remains unmodified, while the top inlet is subjected to reduced nozzle pressure ratios with a differential factor DF = 10%, 25% and 50%. For the case of NPR = 5, this results in NPR_{Top} = 4.5, 3.75 and 2.5 against DF = 10%, 25% and 50%, respectively. Accordingly, for the case of NPR = 50, it results in NPR_{Top} = 45, 37.5 and 25. While, for the case of NPR = 200, NPR_{Top} = 150 and 100 against DF = 25% and 50%, respectively;

Table 1 – DIMENSIONS OF COMPUTED NOZZLE

Quantity	Symbol	Value
Aerospike Nozzle Exit Area	A_e	5003.21 mm^2
Width of Single Throat	b	77.55 mm
Height of Single Throat	h_t	2.55 mm
Area of Both Throats	A_t	395.51 mm^2
Width to Height Ratio, of the Throat	b/h_t	30.41
Aerospike Nozzle Area Ratio	A_e/A_t	12.65

(a) DF = 0%   (b) DF = 25%   (c) DF = 50%
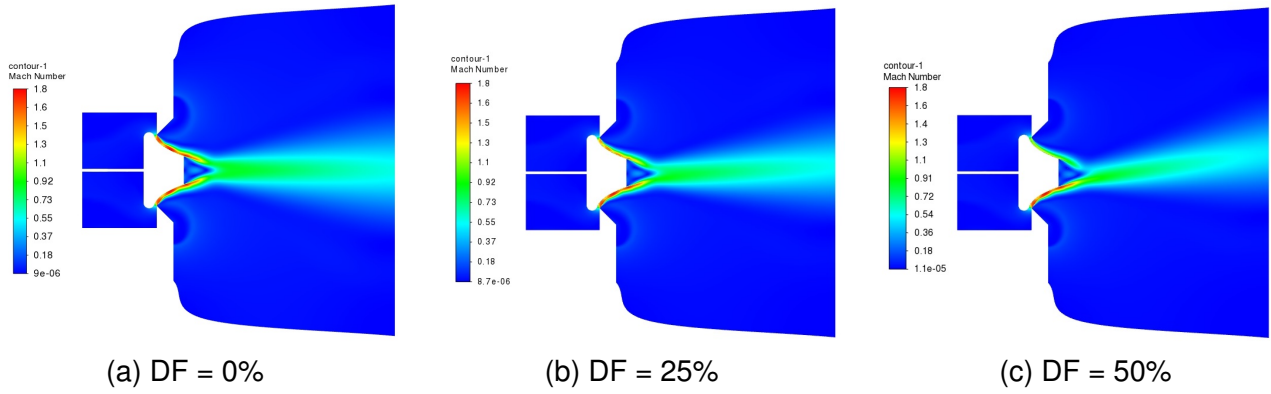
Figure 3 – Mach contours at NPR = 5 for different DF-values

(a) DF = 0%   (b) DF = 25%   (c) DF = 50%
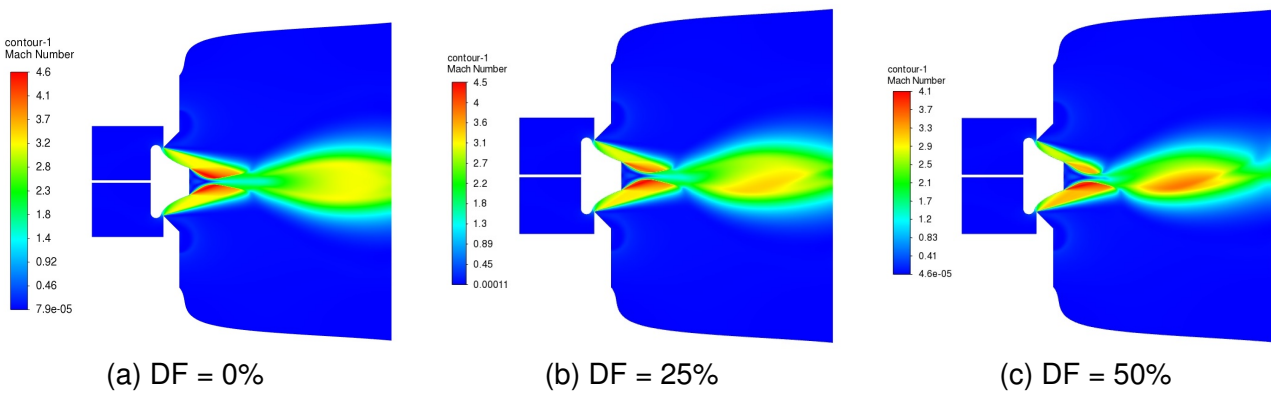
Figure 4 – Mach contours at NPR = 50 for different DF-values
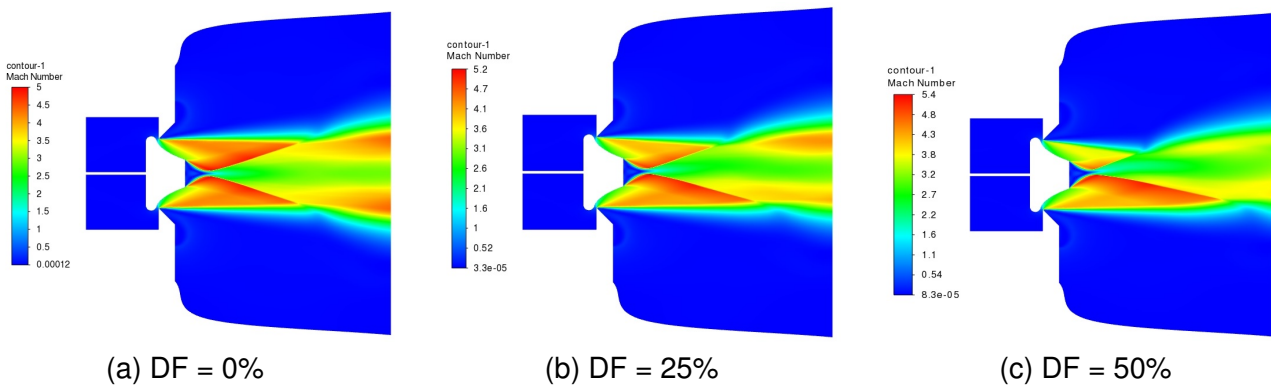

(a) DF = 0%   (b) DF = 25%   (c) DF = 50%

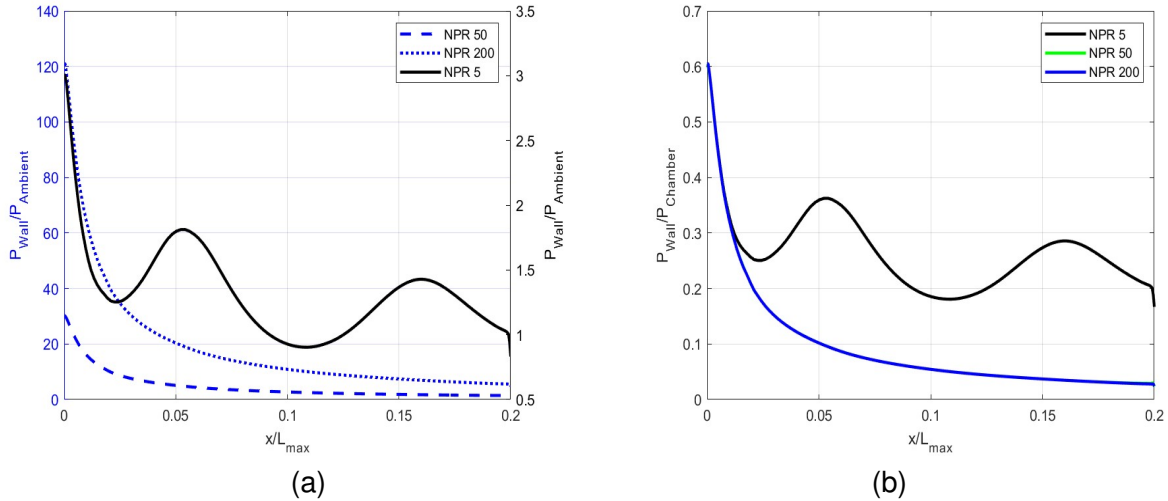Figure 5 – Mach contours at NPR = 200 for different DF-values

Figure 6 – Normalized pressure distribution P_w/P_{amb} **(a)** and P_w/P_c **(b)** on the upper and lower surfaces of LASN20 plug without differential throttling (DF = 0%)

The types of boundaries are pressure inlets, pressure outlets and walls. Ambient pressure, P_{amb}, is considered as 101325 Pascal (Pa), and have been selected according to ref.[19].

3. Numerical Results

Computational results are presented in this section. One of the important engineering tool is the pressure distribution which gives insight into the developed flowfield. Therefore, the main results are processed in the form of Mach number contours for complete domain and absolute static pressure distribution over the plug surfaces.

In case of symmetric mode of nozzle operation, for all three NPR values, these pressure distributions have been normalized with respect to both ambient pressure and their respective maximum values of pressure in the chamber. While, for the case of asymmetric mode of nozzle operation, at all differential-factors, plug pressure distributions have been normalized with respect to their respective chamber pressures at DF = 0% for all NPR values.

3.1 Flowfield Analysis

For NPR = 5, 50 and 200, at both non-differential and differential throttling configurations, figures 3, 4 and 5 illustrate the flowfield in terms of Mach number around the LASN20 plug, respectively. And at these values of NPR, the maximum Mach number in the flowfields is 1.8, 4.6 and 5.4, respectively.

Since exhaust from either profiled-side of the linear aerospike nozzle is going downstream independently, it interacts with each other just at the truncated base. When the flowfield is in differentially-throttled configuration, both parts of the exhaust are with different flow properties and their subsequent downstream interaction results in skewed exhaust plume to the side of chamber with lower NPR. This is the flowfield indication of thrust vectoring that has happened because of the employment of differential throttling which had resulted in difference of pressure distribution over either sides of the plug. Figure 3 shows the presence of compression and expansion waves around the plug and the subsonic region at its base and also the complex nature of interaction of these waves after the base in the attachment zone of the flowfield, whereas, recompression does not occur over the surfaces of the plug for NPR = 50 and 200 as evident in figures 4 and 5, respectively.

Figure 6 shows the distributions of pressure ratios ((a) P_w/P_{amb} and (b) P_w/P_c) along upper and lower contoured surfaces of LASN20 plug, starting from throat of the sub-nozzle and ending at the truncated base. The right y-axis is for NPR = 5. For NPR = 5, both expansion and compression waves create the pressure distribution over the plug surfaces and it has expanded near to ambient pressure at the lip of the base. Observing left y-axis, however, for NPR = 50 and NPR = 200, there are no compression
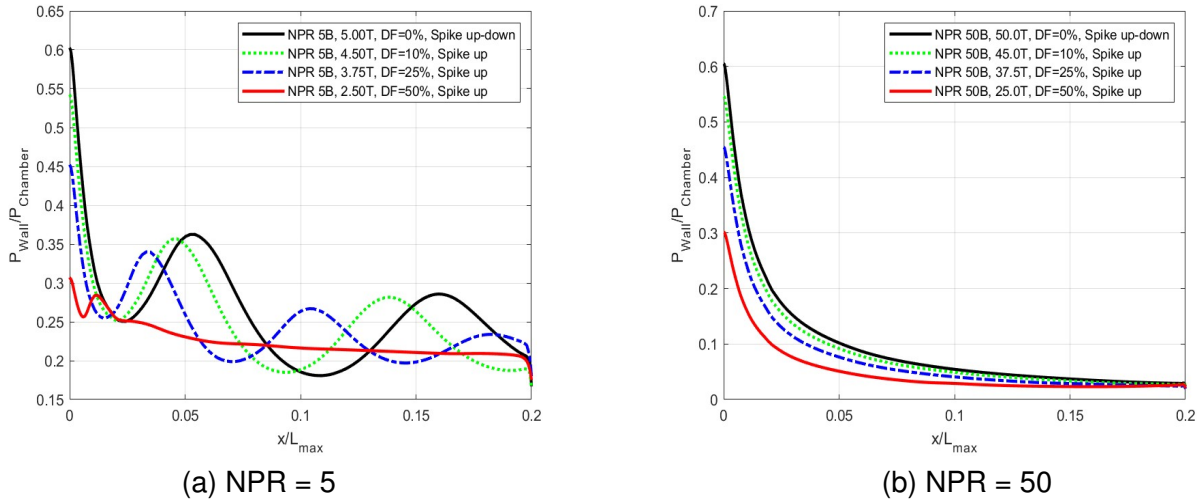
(a) NPR = 5

(b) NPR = 50

Figure 7 – Normalized pressure distribution P_w/P_c over upper and lower surfaces of LASN20 plug with differential throttling

waves affecting the pressure distribution over the plug and the gradual pressure-decrease is only affected by the expansion wave. For each NPR, this pressure distribution is unique with respect to ambient pressure. Moreover, for NPR = 50 and 200, the distribution of pressure ratio of P_w/P_c remains unchanged and gives a common distribution.

In figures 7(a) and (b), distribution of pressure ratio P_w/P_c, obtained at different values of differential factor, is reported for NPR = 5 and 50, respectively. Again, it is evident from these figures that the flowfield over the plug is composed of compression and expansion waves for NPR = 5; while for NPR = 50, it is characterized by only the initial expansion wave, which generates at the tip of the cowl near the throat of the sub-nozzle. During the asymmetric operation of the nozzle at NPR = 5, the flowfields over the lower and upper surfaces of the plug are independent of each other as they are developed due to different values of nozzle pressure ratios and figure 7(a) quite clearly predicts the varying flowfield, with upstream shift of expansion and re-compression waves and subsequent variation in their strengths. In the same manner, for the case of NPR = 50, figure 7(b) also predicts the upstream shift of incident rays of expansion-fan over the plug as NPR decreases.

4. Conclusions

Flowfield, in a differentially-throttled linear aerospike nozzle, is investigated computationally for NPR = 5, 50 and 200 at different values of NPR differential-factor (DF = 0%, 10%, 25% and 50%), where DF = 0% represents the base-case of non-differentially throttled nozzle.

The numerical results accurately characterize the flowfield around the linear aerospike nozzle in terms of Mach number contours and pressure distribution over the plug surfaces, for both modes of its operation, i.e., symmetric and asymmetric. This study helps in building a database of computational results for such modes of operation of linear aerospike nozzle.

5. Contact Author Email Address

jehangir.hassan@polito.it

6. Copyright Statement

Nomenclature

$LASN20$ = Linear AeroSpike Nozzle with 20% plug of its ideal length
D_e = Exit Diameter
T = Top
B = Bottom
P_{amb} = Ambient Pressure
P_c = Chamber Static Pressure
P^o_{Top} = Top-Inlet Total Pressure
P^o_{Bottom} = Bottom-Inlet Total Pressure
P_w = Wall Pressure
NPR = Nozzle Pressure Ratio, P_c/P_{amb}
NPR_{Top} = Nozzle Pressure Ratio w.r.t. Top Portion of Chamber, P^o_{Top}/P_{amb}
NPR_{Bottom} = Nozzle Pressure Ratio w.r.t. Bottom Portion of Chamber, P^o_{Bottom}/P_{amb}
DF = Differential throttling factor, where, $DF = 100 \cdot (1 - \frac{\text{NPR}_{Top}}{\text{NPR}_{Bottom}})$

References

[1] Larrimer BI *Beyond Tube-and-Wing*. NASA, 2020.

[2] Asbury S.C., Capone F.J.. High-Alpha Vectoring Characteristics of the F-18/HARV. *Journal of Propulsion and Power.* 1994;10(1):116-121.

[3] Yagle P.J., Miller D.N., Ginn K.B., Hamstra J.W.. Demonstration of Fluidic Throat Skewing for Thrust Vectoring in Structurally Fixed Nozzles. *ASME Journal of Engineering for Gas Turbines and Power.* 2001;123(3):502–507.

[4] Deere K.A.. Summary of Fluidic Thrust Vectoring Research Conducted at NASA Langley Research Center. *21st AIAA Applied Aerodynamics Conference, Orlando, Florida, AIAA Paper 2003-3800.* 2003; : .

[5] Ferlauto M., Marsilio R.. A Numerical Method for the Study of Fluidic Thrust Vectoring. *Advances in Aircraft and Spacecraft Science.* 2016;3(4):367–378.

[6] Warsop C., Crowther W., Forster M.. NATO AVT-239 Task Group: Supercritical Coanda based Circulation Control and Fluidic Thrust Vectoring. *Paper AIAA 2019-0044, AIAA Scitech 2019 Forum,San Diego, CA.* 2019; : .

[7] Li L., Hirota M., Ouchi K., Saito T.. Evaluation of fluidic thrust vectoring nozzle via thrust pitching angle and thrust pitching moment. *Shock Waves.* 2017;27(1):53-61.

[8] Rocketdyne. *Interim report, Advanced Aerodynamic Spike Configurations*. Rocketdyne Advanced Projects, Large Engines, AFRPL, November 1966.

[9] O'Brien CJ. *Unconventional nozzle tradeoff study - Final Report*. Aerojet Liquid Rocket Company, for NASA, July 1979.

[10] Gagliardi M, Fadigati L, Souhair M, Ponti F. Validation of a numerical strategy to simulate the expansion around a plug nozzle. *Aeronautics and Astronautics - AIDAA XXVII International Congress*, Materials Research Proceedings 37, 695-698, 2023.

[11] Soman S, Suryan A, Nair PP, Kim HD. Numerical Analysis of Flowfield in Linear Plug Nozzle with Base Bleed. *Journal of Spacecraft and Rockets*, Vol. 58, No. 6, 9 Aug 2021.

[12] Ferlauto M, Ferrero A, Marsicovetere M, Marsilio R. Differential Throttling and Fluidic Thrust Vectoring in a Linear Aerospike. *International Journal of Turbomachinery Propulsion and Power*, 6(2), 2021.

[13] Hamedi-Estakhrsar MH, Ferlauto M, Mahdavy-Moghaddam H. Numerical study of secondary mass flow modulation in a Bypass Dual-Throat Nozzle. *Journal of Aerospace Engineering*, Vol. 235(4), pp 488–500, 2021.

[14] Marsilio R, Resta E, Di Cicca GM, Ferlauto M. Thrust Vectoring using Differential Throttling in Axisymmetric Aerospike Nozzle. *AIAA SciTech Forum*, Orlando, FL, 8–12 January 2024.

[15] Eilers S.D., Wilson M.D., Whitmore S.A., Peterson Z.W.. Side Force Amplification on an Aerodynamically Thrust Vectored Aerospike Nozzle. *AIAA paper 2011-5531, 47th AIAA/ASME/SAE/ASEE Joint Propulsion Conference & Exhibit, San Diego, CA.* 2011; : .

[16] Geron M, Paciorri R, Nasuti F, Sabetta F. Flowfield analysis of a linear clustered plug nozzle with round-to-square modules. *Aerospace Science and Technology*, Vol. 11, pp 110-118, 2007.

[17] *Ansys Fluent Theory Guide*. Release 2022 R2, Ansys Inc., July 2022.

[18] Spalart P.R., Johnson F.T., Allmaras S.R.. Modifications and Clarifications for the Implementation of the Spalart-Allmaras Turbulence Model. *paper ICCFD7-1902, seventh International Conference on Computational Fluid Dynamics (ICCFD7), Big Island, Hawaii.* 2012;:1-11.

[19] Poinsot T.J., Lele S.K.. Boundary conditions for direct simulations of compressible viscous reacting flows. *Journal of Computational Physics.* 1992;101:104–129.

[20] Tian C., Lu Y.. Turbulence Models of Separated Flow in Shock Wave Thrust Vector Nozzle. *Engineering Applications of Computational Fluid Mechanics.* 2013;7(2):182–192.

[21] Ferlauto M., Marsilio R.. Computational Investigation of Injection Effects on Shock Vector Control Performance. *Paper AIAA-2018-4934, 54th AIAA/SAE/ASEE Joint Propulsion Conference, Cincinnati, OH.* 2018;:1–10.

[22] Noori S, Shahrokhi A. Flow Field Characteristics of an Aerospike Nozzle Using Different Turbulence Models. *Journal of Aerospace Science and Technology, JAST*, Research Note, Vol. 8(2), pp 127–133, 2011.

[23] Angelino G, Approximate method for plug nozzle design, *AIAA Journal*, vol. 2, no. 10, pp 1834-1835, 1964.

[24] Di Cicca G M, Hassan J, Resta E, Marsilio R, Ferlauto M. Experimental Characterization of a Linear Aerospike Nozzle Flow. *IEEE Workshop on Metrology for Aerospace 2023*, Milan, Italy, 2023.

[25] Di Cicca G M, Resta E, Marsilio R, Hassan J, Ferlauto M. A Framework for Testing Differential Throttling in Linear Aerospike Nozzle . *IEEE Workshop on Metrology for Aerospace 2024*, Lublin, Poland, 2024.